Available online at www.sciencedirect.com
SCIENCE DIRECT®
Composites Science and Technology 64 (2004) 129–144
COMPOSITES SCIENCE AND TECHNOLOGY
www.elsevier.com/locate/compscitech

The effect of recycling on the time-dependent behavior of polycarbonate reinforced with short glass fibers

A.D. Drozdov*, A. Al-Mulla, R.K. Gupta

Department of Chemical Engineering, West Virginia University, PO Box 6102, Morgantown, WV 26506, USA

Received 7 January 2003; received in revised form 22 May 2003; accepted 23 May 2003

Abstract

Observations are reported on virgin, recycled and a mixture of virgin and recycled polycarbonates reinforced with various amounts of short glass fibers (1) in tensile tests with a constant strain rate and (2) in oscillatory torsion tests at room temperature. A constitutive model is developed for the viscoelastic and viscoplastic behavior of a polymer composite with a glassy matrix. The composite is treated as an equivalent ensemble of meso-regions linked with each other. With reference to the theory of cooperative relaxation, the viscoelastic response is attributed to rearrangement of meso-domains. The viscoplastic behavior reflects sliding of meso-regions with respect to each other. The rate of sliding is proportional to the rate of macro-deformation. Constitutive equations for isothermal three-dimensional deformation with small strains are derived by using the laws of thermodynamics. The stress–strain relations are determined by five adjustable parameters that are found by fitting the experimental data. The study concentrates on the effects of filler content and recycling of the host matrix on the mechanical properties of composites.

Keywords: A: Polymer-matrix composites (PMCs); A: Short-fiber composites; B: Mechanical properties; C: Anelasticity; C: Complex moduli

1. Introduction

This paper is concerned with the comparative study of the viscoelastic and viscoplastic responses of virgin and recycled polycarbonates reinforced with short glass fibers. We concentrate on the mechanical behavior of polymer composites at isothermal deformation with small strains observed in uniaxial tensile tests with a constant strain rate and oscillatory torsion tests at ambient temperature.

In-plant recycling of polymers and polymer composites and recycling of post-consumer plastic waste have been a focus of attention in the past decade [1–18], which may be explained by (i) limited natural resources, (ii) rising waste-handling costs, and (iii) environmental regulations related to land-filling and incineration of plastics. Post-consumer plastic waste is characterized by (i) alteration of the structure of chains and topology of polymeric networks driven by oxidative degradation, and (ii) the presence of incompatible polymers (residual additives) and inorganic inclusions [19,20]. Thermo-oxidative degradation of end-of-life polymers is unavoidable, but its effect on the viscoelastic and viscoplastic behavior of polymers remains the subject of debate.

One natural way to improve mechanical properties of recycled polymers is to reinforce them with short glass fibers. In the past decade, the viscoelastic and viscoplastic responses of amorphous and semicrystalline polymers filled with short glass fibers (with the aspect ratio of the order of 10^2) have been investigated in Refs. [21–32], to mention a few. The interest to this subject may be explained by wide-range industrial applications of thermoplastics reinforced with short glass fibers, in particular, in automotive and electronics industries.

To develop stress–strain relations, we apply a method of homogenization [33], according to which a sophisticated micro-structure of a polymer composite is replaced by an equivalent phase whose response captures the most important features of the mechanical behavior of the composite. A network of macromolecules is chosen as the equivalent phase. With reference to the theory of cooperative relaxation [34], the network is assumed to be strongly heterogeneous. It is

* Corresponding author. Tel.: +1-304-293-211; fax: +1-304-293-4139.
E-mail address: aleksey.drozdov@mail.wvu.edu (A.D. Drozdov).

0266-3538/$ - see front matter © 2003 Elsevier Ltd. All rights reserved.
doi:10.1016/S0266-3538(03)00232-X

thought of as an ensemble of meso-regions (MRs) or cooperatively rearranged domains linked with each other. A meso-domain is treated as a globule consisting of scores of neighboring chains [35] that change their positions simultaneously due to large-angle reorientation of strands. The presence of cooperatively relaxing regions in amorphous polymers (observed as "isolated cohesive regions" in polymer glasses) was experimentally confirmed by low-frequency Raman scattering [36]. The characteristic length of a meso-region is estimated as a few nanometers [37,38].

In the stress-free state, all meso-domains are connected with one another by links which ensure that micro-strains in MRs coincide with the macro-strain. The links are associated with "less cohesive spaces between more cohesive domains" [36], and they reflect the effects of entanglements and van der Waals forces between macromolecules in the host matrix, as well as the influence of glass fibers on the mechanical response of a composite. Under deformation, some links break, which results in mutual displacements of meso-regions.

To describe displacements of MRs with respect to each other, we introduce a linear relation between the strain rate for macro-deformation and the rate for sliding of meso-regions. This approach allows the number of adjustable parameters in the constitutive equations to be reduced noticeably. A similar relationship (for one-dimensional deformation) has been proposed in our recent work on the viscoplastic behavior of semicrystalline polymers [39].

The objective of this study is three-fold:

1. To report experimental data on virgin, recycled and a mixture of virgin and recycled polycarbonates reinforced with various amounts of short glass fibers in uniaxial tensile tests with a constant strain rate and in oscillatory torsion tests with a wide range of frequencies.
2. To derive constitutive equations for three-dimensional viscoelastic and viscoplastic responses of an equivalent ensemble of meso-domains and to determine adjustable parameters in the stress–strain relations by fitting the observations.
3. To analyze the influence of recycling and the effect of concentration of short glass fibers on the time-dependent behavior of polymer composites.

The exposition is organized as follows. The experimental procedure is described in Section 2. Kinetic equations for thermally-induced rearrangement of meso-domains are developed in Section 3. Sliding of meso-regions with respect to each other is discussed in Section 4. Constitutive equations for the time-dependent response of an ensemble of meso-regions are derived in Section 5 by using the laws of thermodynamics. The stress–strain relations are simplified for uniaxial tension and simple shear in Sections 6 and 7. Adjustable parameters in the governing equations are found in Section 8 by matching the experimental data. A brief discussion of our findings is provided in Section 9. Some concluding remarks are formulated in Section 10.

2. Experimental procedure

As short glass fibers are difficult and hazardous to handle, polymer composites reinforced with various amounts of filler were prepared by blending neat polycarbonate with polycarbonate with a high concentration of fibers. As the neat polymers, virgin polycarbonate Lexan HF1110 (purchased from GE Plastics) and recycled polycarbonate donated by MBA Polymers are used, and as a polymer reinforced with a high concentration of fibers (40 wt.%) we employed polycarbonate RTP307 (purchased from RTP Company). According to the suppliers, polycarbonate HF1110 and the host matrix of polycarbonate RTP307 have similar molecular weights, which implies that the difference in their mechanical responses may be disregarded.

To prepare samples with various concentrations of glass fibers ($\phi = 0$, 5, 10, 15 and 20 wt.%), a fixed amount of the neat polycarbonate was blended with an appropriate amount of RTP307. To receive mass M of the final product, we mixed mass M_1 of RTP307 with mass $M_2 = M - M_1$ of the neat polycarbonate. The mass of glass gibers in the mixture was 0.4 M_1, and their concentration was 0.4 M_1/M. Equating this quantity to ϕ, the content of RTP307 in the blend was found, $M_1 = 0.025\ \phi M$. Three types of polymer composites were prepared:

1. Virgin polycarbonate, where mass, M_2, of polycarbonate Lexan HF1110 was blended with mass M_1 of polycarbonate RTP307.
2. Recycled polycarbonate, where mass M_2 of recycled polycarbonate was blended with mass M_1 of polycarbonate RTP307.
3. A mixture of virgin and recycled polycarbonates, where equal amounts, 0.5 M_2, of virgin polycarbonate Lexan HF1110 and recycled polycarbonate were blended with mass M_1 of polycarbonate RTP307.

Granules were dried in an oven at the temperature $T = 120$ °C for 12 h, pellets were mixed by vigorous shaking and mechanically blended in a twin-screw extruder (Brabender Instruments, Inc.) with a screw rate of 50 rpm and temperatures in the extruder barrel of 240, 270, 285 and 280 °C from hopper to die, respectively. No degradation of the polymeric matrices was

observed. The strands from the extruder were cooled in a water bath, cut with a pelletizer, and dried in an oven at 120 °C for 12 h. Specimens for mechanical tests were molded by using injection molding machine BA1000-CDC (Battenfeld).

Sizes of fibers in the composites were determined visually by burning samples and measuring the fiber lengths on a microscope slide (500 fibers). The average length was 0.23 mm, and its standard deviation was 0.14 mm. The average aspect ratio of short glass fibers was about 20.

Dumbbell specimens for tensile tests were prepared in accordance with ASTM D638 specification. Tensile tests were performed by using a 100 kN Instron machine model 8501 with a cross-head speed of 5 mm/min at room temperature. The chosen cross-head speed (that corresponded to the strain rate $\dot{\varepsilon} = 9.80 \times 10^{-4}$ s^{-1}) ensured nearly isothermal experimental conditions. It also allowed the viscoelastic effects to be disregarded. The duration of loading before the onset of neck was less than 1 min, while the decrease in stress in polycarbonate specimens during this period observed in relaxation tests in the sub-yield region of deformations at room temperature does not exceed a few percent [40,41].

The tensile force was measured by a standard load cell. The longitudinal strain was determined by using a strain gauge affixed to the mid-point of a specimen. The engineering stress, σ, was determined as the ratio of the axial force to the cross-sectional area of a stress-free specimen. The series of tensile tests consisted of five experiments on specimens filled with $\phi = 0$, 5, 10, 15 and 20 wt.% of short glass fibers. To minimize the effect of physical aging, tensile tests were carried out a few days after preparation of samples.

The engineering stress, σ, is plotted versus the engineering strain, ε, in Figs. 1–3 (only the data obtained before the onset of neck are presented). These figures show that the stress, σ, strongly increases with strain, ε, and the stress–strain curves noticeably differ from straight lines (corresponding to the stress–strain diagrams of an elastic medium). Given a strain, ε, the stress monotomcally increases with the content of fibers, ϕ. The strain, ε_n, corresponding to the point where a neck is formed decreases with the fraction of filler.

Dynamic tests were performed by using RMS-800 rheometric mechanical spectrometer in rectangular torsion mode (the samples were used with length 45.5 mm, width 13.0 mm and thickness 3.0 mm). The shear

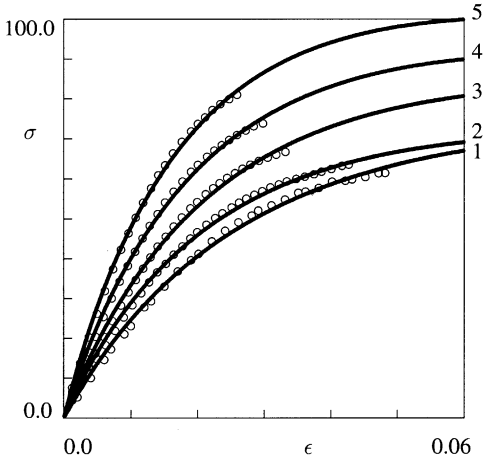

Fig. 2. The stress σ MPa versus strain ε. Circles: experimental data in tensile tests with a strain rate of 5 mm/min on recycled polycarbonate reinforced with ϕ wt.% of short glass fibers. Solid lines: results of numerical simulation. Curve 1: $\phi = 0.0$. Curve 2: $\phi = 5.0$. Curve 3: $\phi = 10.0$. Curve 4: $\phi = 15.0$. Curve 5: $\phi = 20.0$.

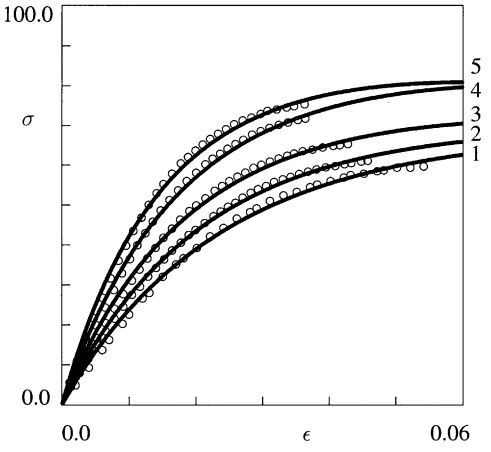

Fig. 1. The stress σ MPa versus strain ε. Circles: experimental data in tensile tests with a strain rate of 5 mm/min on virgin polycarbonate reinforced with ϕ wt.% of short glass fibers. Solid lines: results of numerical simulation. Curve 1: $\phi = 0.0$. Curve 2: $\phi = 5.0$. Curve 3: $\phi = 10.0$. Curve 4: $\phi = 15.0$. Curve 5: $\phi = 20.0$.

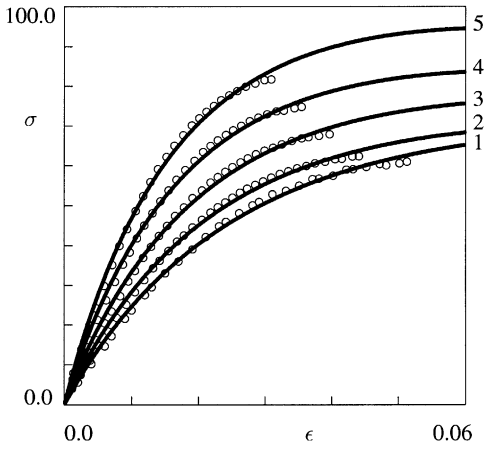

Fig. 3. The stress σ MPa versus strain ε. Circles: experimental data in tensile tests with a strain rate of 5 mm/min on mixture of virgin and recycled polycarbonates reinforced with ϕ wt.% of short glass fibers. Solid lines: results of numerical simulation. Curve 1: $\phi = 0.0$. Curve 2: $\phi = 5.0$. Curve 3: $\phi = 10.0$. Curve 4: $\phi = 15.0$. Curve 5: $= 20.0$.

storage modulus, G', and the shear loss modulus, G'', are measured in oscillatory tests (the frequency–sweep mode) with the fixed strain amplitude of 0.1% and various frequencies, ω, in the range from 0.01 to 100 rad/s. The temperature in the chamber was controlled with a standard thermocouple. It indicated that the temperature remained constant at frequencies up to 20 rad/s and strongly increased at higher frequencies.

The storage and loss moduli are plotted versus the logarithm ($\log = \log_{10}$) of frequency, ω, in Figs. 4–9. These figures show that for any concentration of glass fibers under consideration, the storage modulus, G', is weakly affected by frequency (it slightly increases with $\log \omega$), whereas the loss modulus, G'', pronouncedly decreases with $\log \omega$. The rate of decrease in G'' grows with the filler content. Given a frequency, ω, both moduli noticeably increase with concentration of glass fibers, ϕ.

Our aim now is to develop a constitutive model that can adequately describe the experimental data depicted in Figs. 1 to 9.

3. Rearrangement of meso-regions

With reference to the theory of cooperative relaxation [34], the viscoelastic response of an ensemble of meso-domains it thought of as a sequence of rearrangement

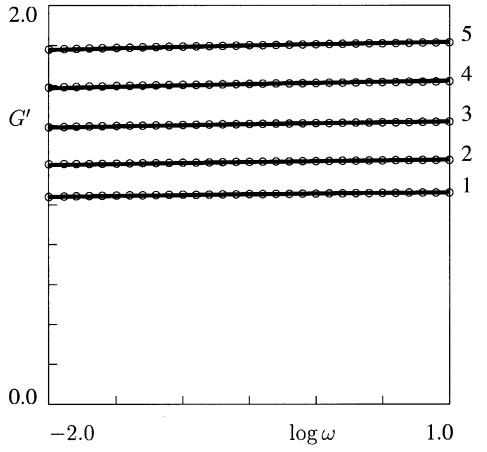

Fig. 4. The storage modulus G' GPa versus frequency ω rad/s. Circles: experimental data in oscillatory torsion tests on virgin polycarbonate reinforced with ϕ wt.% of short glass fibers. Solid lines: results of numerical simulation. Curve 1: $\phi = 0.0$. Curve 2: $\phi = 5.0$. Curve 3: $\phi = 10.0$. Curve 4: $\phi = 15.0$. Curve 5: $\phi = 20.0$.

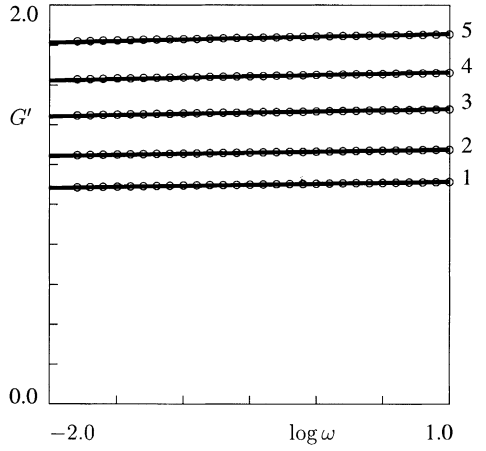

Fig. 6. The storage modulus G' GPa versus frequency ω rad/s. Circles: experimental data in oscillatory torsion tests on recycled polycarbonate reinforced with ϕ wt.% of short glass fibers. Solid lines: results of numerical simulation. Curve 1: $\phi = 0.0$. Curve 2: $\phi = 5.0$. Curve 3: $\phi = 10.0$. Curve 4: $\phi = 15.0$. Curve 5: $\phi = 20.0$.

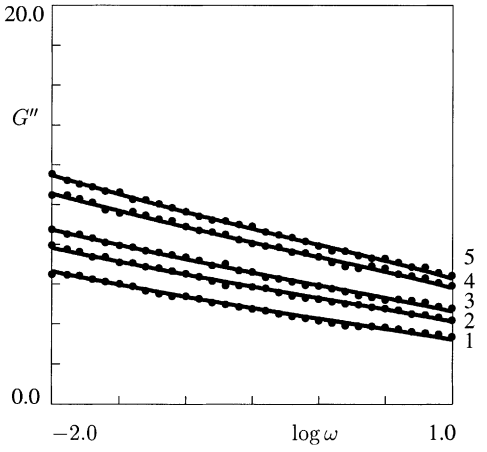

Fig. 5. The loss modulus G'' MPa versus frequency ω rad/s. Circles: experimental data in oscillatory torsion tests on virgin polycarbonate reinforced with ϕ wt.% of short glass fibers. Solid lines: results of numerical simulation. Curve 1: $\phi = 0.0$. Curve 2: $\phi = 5.0$. Curve 3: $\phi = 10.0$. Curve 4: $\phi = 15.0$. Curve 5: $\phi = 20.0$.

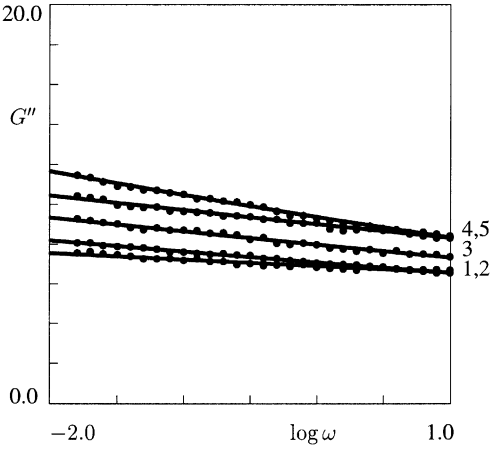

Fig. 7. The loss modulus G'' MPa versus frequency ω rad/s. Circles: experimental data in oscillatory torsion tests on recycled polycarbonate reinforced with ϕ wt.% of short glass fibers. Solid lines: results of numerical simulation. Curve 1: $\phi = 0.0$. Curve 2: $\phi = 5.0$. Curve 3: $\phi = 10.0$. Curve 4: $\phi = 15.0$. Curve 5: $\phi = 20.0$.

events for individual MRs. To describe the rearrangement process, we model a MR as a point trapped in its potential well on the energy landscape [35]. At random instants, the point hops from the bottom level of its potential well to higher energy levels as it is activated by thermal fluctuations (see Fig. 1 in [42]). According to the transition-state theory [43], stresses in a meso-region totally relax when it reaches some liquid-like (reference) level in a hop.

The depth of a potential well with respect to the reference energy level is determined by its energy $\upsilon > 0$. Denote by N the total number of MRs per unit mass of the ensemble, and by $p(\upsilon)$ the distribution function for traps with various energies. The kinetics of rearrangement is entirely determined by the function $n(t, \tau, \upsilon)$ that equals the number of MRs (at time $t \geqslant 0$) trapped in cages with potential energy υ that have last rearranged before instant $\tau \in [0, t]$. The quantity $n(t, t, \upsilon)$ equals the number of meso-domains (per unit mass) located in traps with energy υ at time t,

$$n(t, t, \upsilon) = Np(\upsilon) \tag{1}$$

The amount $\varphi(\tau, \upsilon)d\tau$, where

$$\varphi(\tau, \upsilon) = \frac{\partial n}{\partial \tau}(t, \tau, \upsilon)|_{t=\tau}, \tag{2}$$

equals the number of MRs (per unit mass) trapped in cages with energy υ that rearranged within the interval $[\tau, \tau + d\tau]$. The quantity

$$\frac{\partial n}{\partial \tau}(t, \tau, \upsilon)d\tau$$

is the number of these meso-domains that have not rearranged during the interval $[\tau + d\tau, t]$. The amount

$$-\frac{\partial n}{\partial \tau}(t, 0, \upsilon)dt$$

is the number of MRs (per unit mass) that rearrange (for the first time) within the interval $[t, t + dt]$, while the quantity

$$-\frac{\partial^2 n}{\partial t \partial \tau}(t, \tau, \upsilon)dtd\tau$$

is the number of meso-regions (per unit mass) that have rearranged within the interval $[\tau, \tau + d\tau]$, did not reach the liquid-like level during the interval $[\tau + d\tau, t]$, and rearranged once more within the interval $[t, t + dt]$.

Let $q(u)du$ be the probability for a MR to reach (in a hop) the energy level belonging to the interval $[u, u + du]$. Referring to [44], we adopt the exponential distribution

$$q(u) = \beta \exp(-\beta u),$$

where β is a material constant. The probability to reach the reference state in an arbitrary hop reads

$$q_0(\upsilon) = \int_{\upsilon}^{\infty} q(u)du = \exp(-\beta\upsilon).$$

Denote by γ the attempt rate (the average number of hops in a cage per unit time). The rate of rearrangement, Γ, is defined as the product of the attempt rate, γ, by the probability of reaching the liquid-like level in a hop q_0,

$$\Gamma(\upsilon) = \gamma \exp(-\beta\upsilon).$$

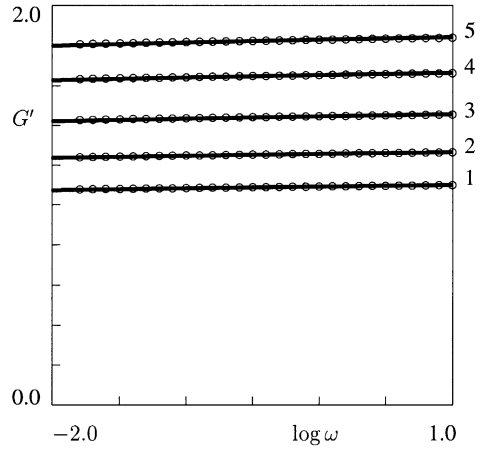

Fig. 8. The storage modulus G′ GPa versus frequency ω rad/s. Circles: experimental data in oscillatory torsion tests on mixture of virgin and recycled polycarbonates reinforced with ϕ wt.% of short glass fibers. Solid lines: results of numerical simulation. Curve 1: $\phi = 0.0$. Curve 2: $\phi = 5.0$. Curve 3: $\phi = 10.0$. Curve 4: $\phi = 15.0$. Curve 5: $\phi = 20.0$.

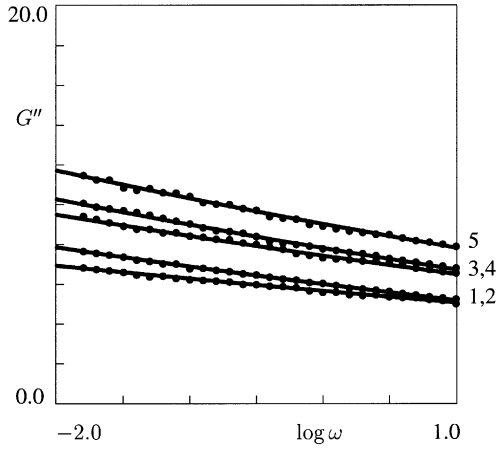

Fig. 9. The loss modulus G'' MPa versus frequency ω rad/s. Circles: experimental data in oscillatory torsion tests on mixture of virgin and recycled polycarbonates reinforced with ϕ wt.% of short glass fibers. Solid lines: results of numerical simulation. Curve 1: $\phi = 0.0$. Curve 2: $\phi = 5.0$. Curve 3: $\phi = 10.0$. Curve 4: $\phi = 15.0$. Curve 5: $\phi = 20.0$.

Without loss of generality, we set $\beta=1$ in this equality, which implies that the potential energies of traps are measured in units of β^{-1},

$$\Gamma(\upsilon)=\gamma\exp(-\upsilon). \tag{3}$$

The rate of rearrangement, Γ, is determined as the ratio of the number of MRs rearranged per unit time to the total number of meso-domains. Applying this definition to MRs that rearrange for the first time within the interval $[t,t+dt]$ and to those that have previously rearranged during the interval $[\tau,\tau+d\tau]$, we arrive at the differential equations

$$\frac{\partial n}{\partial t}(t,0,\upsilon)=-\Gamma(\upsilon)n(t,0,\upsilon),$$
$$\frac{\partial^2 n}{\partial t\partial\tau}(t,\tau,\upsilon)=-\Gamma(\upsilon)\frac{\partial n}{\partial\tau}(t,\tau,\upsilon). \tag{4}$$

Integration of Eq. (4) with initial conditions (1) (where we set $t=0$) and (2) implies that

$$n(t,0,\upsilon)=Np(\upsilon)\exp[-\Gamma(\upsilon)t], \tag{5}$$

$$\frac{\partial n}{\partial\tau}(t,\tau,\upsilon)=\varphi(\tau,\upsilon)\exp[-\Gamma(\upsilon)(t-\tau)]. \tag{6}$$

To exclude the function $\varphi(t,\upsilon)$ from Eq. (6), we use the identity

$$n(t,t,\upsilon)=n(t,0,\upsilon)+\int_0^t\frac{\partial n}{\partial\tau}(t,\tau,\upsilon)d\tau. \tag{7}$$

Substitution of expressions (1) and (6) into Eq. (7) results in

$$Np(\upsilon)=Np(\upsilon)\exp[-\Gamma(\upsilon)t]+\int_0^t\varphi(\tau,\upsilon)\exp[-\Gamma(\upsilon)(t-\tau)]d\tau. \tag{8}$$

The solution of Eq. (8) reads

$$\varphi(t,\upsilon)=N\Gamma(\upsilon)p(\upsilon).$$

Combining this equality with Eq. (6), we find that

$$\frac{\partial n}{\partial\tau}(t,\tau,\upsilon)=N\Gamma(\upsilon)p(\upsilon)\exp[-\Gamma(\upsilon)(t-\tau)]. \tag{9}$$

Eqs. (3), (5) and (9) entirely determine the kinetics of rearrangement of meso-regions in an ensemble.

4. Sliding of meso-domains

Deformation of a specimen induces breakage of links between meso-regions, which causes sliding of MRs with respect to each other. Denote by $\hat{\varepsilon}$ the macro-strain tensor and by $\hat{\varepsilon}_{\rm p}$ the plastic strain tensor that reflects sliding of meso-domains. An increase in the macro-strain, $\hat{\varepsilon}$, by an increment, $d\hat{\varepsilon}$, induces an increase in the plastic strain tensor, $\hat{\varepsilon}_{\rm p}$, by an increment, $d\hat{\varepsilon}_{\rm p}$, that is assumed to be proportional to $d\hat{\varepsilon}$,

$$\frac{{\rm d}\hat{\varepsilon}_{\rm p}}{{\rm d}t}=\alpha\frac{{\rm d}\hat{\varepsilon}}{{\rm d}t}. \tag{10}$$

Eq. (10) differs from conventional flow rules in viscoplasticity of polymers, where the rate of viscoplastic strain is expressed in terms of the stress tensor. This formula is, however, confirmed by the observations that "tensile deformations of polymers ... are strain-controlled" [45]. The coefficient of proportionality, α, is treated as a function of the elastic strain tensor, $\hat{\varepsilon}_{\rm e}$. The latter is conventionally defined as the difference between the macro-strain tensor, $\hat{\varepsilon}$, and the plastic strain tensor, $\hat{\varepsilon}_{\rm p}$,

$$\hat{\varepsilon}_{\rm e}(t)=\hat{\varepsilon}(t)-\hat{\varepsilon}_p(t). \tag{11}$$

To provide an explicit formula for the function $\alpha(\hat{\varepsilon}_{\rm e})$, we introduce the intensity of elastic strain,

$$\varepsilon_{\rm i}=\left(\frac{2}{3}\hat{\varepsilon}'_{\rm e}\colon\hat{\varepsilon}'_{\rm e}\right)^{\frac{1}{2}}, \tag{12}$$

where the prime stands for the deviatoric component of a tensor and the colon denotes convolution. The following conditions are imposed on the dimensionless rate of plastic flow α:

1. the coefficient α vanishes at $\varepsilon_{\rm i}=0$ (no plastic strains are observed at infinitesimal strains);
2. the function $\alpha(\varepsilon_{\rm i})$ monotonically increases with the intensity of elastic strain;
3. this function reaches its limiting value, $\alpha=1$, at relatively large elastic strains (that correspond to a developed plastic flow of MRs, whose rate coincides with the rate of macro-deformation).

To fit experimental data, the following expression for the coefficient α is adopted:

$$\alpha(\varepsilon_{*{\rm i}})=1-\exp\left(-\frac{\varepsilon_{*{\rm i}}}{\varepsilon_*}\right). \tag{13}$$

An important advantage of Eq. (13) is that it contains the only adjustable parameter, the strain, ε_*, that characterizes transition to a developed flow of meso-regions.

5. Constitutive equations

A meso-region is thought of as an incompressible linear elastic medium with the mechanical energy

$$w = \frac{1}{2}\mu\hat{e}' : \hat{e}',$$

where μ is an average rigidity of MR, and $\hat{e}$ is the strain tensor for transition from the natural (stress-free) state of a meso-domain to its deformed state.

As stresses in a MR totally relax when it reaches the liquid-like state, the stress-free configuration of a meso-domain coincides with the deformed configuration of the ensemble at the instant of rearrangement. This means that for meso-regions that have not rearranged before instant $t \geqslant 0$, the strain, $\hat{e}$, is given by

$$\hat{e}(t, 0) = \hat{\varepsilon}_e(t), \tag{14}$$

where $\hat{\varepsilon}_e$ is the elastic strain tensor (which is assumed to coincide for MRs with various activation energies υ). For meso-regions that have last rearranged within the interval $[\tau, \tau + d\tau]$, the strain, $\hat{e}$, reads

$$\hat{e}(t, \tau) = \hat{\varepsilon}_e(t) - \hat{\varepsilon}_e(t). \tag{15}$$

As a polymer composite is treated as an ensemble of MRs linked with each other, the mechanical energy per unit mass of the composite, W, equals the sum of strain energies of meso-domains. Summing the strain energies of MRs with various activation energies, υ, that rearranged at various instants, $\tau \in [0, t]$, using Eqs. (11), (14) and (15), and neglecting the energy of interaction between meso-domains (the latter is taken into account in terms of the incompressibility condition), we find that

$$W(t) = \frac{1}{2}\mu\int_0^\infty \left\{ n(t, 0, \upsilon)\left[\hat{\varepsilon}'(t) - \hat{\varepsilon}'(t)\right] : \left[\hat{\varepsilon}'(t) - \hat{\varepsilon}'_p(t)\right] + \int_0^t \frac{\partial n}{\partial \tau}(t, \tau, \upsilon)\left[\left(\hat{\varepsilon}'(t) - \hat{\varepsilon}'_p(t)\right) - \left(\hat{\varepsilon}'(\tau) - \hat{\varepsilon}'_p(\tau)\right)\right] : \left[\left(\hat{\varepsilon}'(t) - \hat{\varepsilon}'_p(t)\right) - \left(\hat{\varepsilon}'(\tau) - \hat{\varepsilon}'_p(\tau)\right)\right] d\tau \right\} d\upsilon.$$

The derivative of the function $W(t)$ with respect to time reads

$$\frac{dW}{dt}(t) = \hat{A}(t) : \left[\frac{d\varepsilon'}{dt}(t) - \frac{d\varepsilon'_p}{dt}(t)\right] - Y(t), \tag{16}$$

where

$$\hat{A}(t) = \mu\int_0^\infty d\upsilon \left\{ n(t, 0, \upsilon)\left[\hat{\varepsilon}'(t) - \hat{\varepsilon}'_p(t)\right] + \int_0^t \frac{\partial n}{\partial \tau}(t, \tau, \upsilon)\left[\left(\hat{\varepsilon}'(t) - \hat{\varepsilon}'_p(t)\right) - \left(\hat{\varepsilon}'(\tau) - \hat{\varepsilon}'_p(\tau)\right)\right] d\tau \right\}, \tag{17}$$

$$Y(t) = \frac{1}{2}\mu\int_0^\infty d\upsilon \left\{ \frac{\partial n}{\partial t}(t, 0, \upsilon)\left[\hat{\varepsilon}'(t) - \hat{\varepsilon}'_p(t)\right] : \left[\hat{\varepsilon}'(t) - \hat{\varepsilon}'_p(t)\right] + \int_0^t \frac{\partial^2 n}{\partial t \partial \tau}(t, \tau, \upsilon)\left[\left(\hat{\varepsilon}'(t) - \hat{\varepsilon}'_p(t)\right) - \left(\hat{\varepsilon}'(\tau) - \hat{\varepsilon}'_p(\tau)\right)\right] : \left[\left(\hat{\varepsilon}'(t) - \hat{\varepsilon}'_p(t)\right) - \left(\hat{\varepsilon}'(\tau) - \hat{\varepsilon}'_p(\tau)\right)\right] d\tau \right\}. \tag{18}$$

It follows from Eqs. (1), (7) and (17) that

$$\hat{A}(t) = \mu\left\{ N\left[\hat{\varepsilon}'(t) - \hat{\varepsilon}'_p(t)\right] - \int_0^\infty d\upsilon \int_0^t \frac{\partial n}{\partial \tau}(t, \tau, \upsilon)\left[\hat{\varepsilon}'(\tau) - \hat{\varepsilon}'_p(\tau)\right] d\tau \right\}. \tag{19}$$

Substitution of expressions (4) into Eq. (18) results in

$$Y(t) = \frac{1}{2}\mu\int_0^\infty \Gamma(\upsilon) d\upsilon \left\{ n(t, 0, \upsilon)\left[\hat{\varepsilon}(t) - \hat{\varepsilon}'_p(t)\right] : \left[\hat{\varepsilon}(t) - \hat{\varepsilon}'_p(t)\right] + \int_0^t \frac{\partial n}{\partial \tau}(t, \tau, \upsilon)\left[\left(\hat{\varepsilon}'(t) - \hat{\varepsilon}'_p(t)\right) - \left(\hat{\varepsilon}'(\tau) - \hat{\varepsilon}'_p(\tau)\right)\right] : \left[\left(\hat{\varepsilon}'(t) - \hat{\varepsilon}'_p(t)\right) - \left(\hat{\varepsilon}'(\tau) - \hat{\varepsilon}'_p(\tau)\right)\right] d\tau \right\}. \tag{20}$$

Eq. (20) implies that the function $Y(t)$ is non-negative: $\Gamma(\upsilon)$ is positive as the rate of rearrangement of meso-regions, $n(t,0,\upsilon)$ and $\partial n/\partial\tau(t, \tau, \upsilon)$ are non-negative as concentrations of appropriate meso-domains, whereas the convolution of a tensor with itself is always non-negative.

For isothermal deformation of an incompressible medium, the Clausius–Duhem inequality reads

$$Q(t) = -\frac{dW}{dt}(t) + \frac{1}{\rho}\hat{\sigma}'(t) : \frac{d\hat{\varepsilon}'}{dt}(t) \geqslant 0,$$

where Q is internal dissipation per unit mass, ρ is a constant density, $\hat{\sigma}$ stands for the stress tensor. Substituting Eq. (16) into this equality and using Eq. (10), we find that

$$\rho Q(t) = \left[\hat{\sigma}'(t) - \rho(1 - \alpha(\varepsilon_i(t)))\hat{A}(t)\right] : \frac{d\hat{\varepsilon}'}{dt}(t) + \rho Y(t) \geqslant 0. \tag{21}$$

As the function $Y(t)$ is non-negative, dissipation inequality (21) is satisfied for an arbitrary program of loading, provided that the expression in square brackets vanishes. This condition together with Eqs. (9) and (19) results in the stress–strain relation

$$\hat{\sigma}(t) = -P(t)\hat{I} + 2G[1-\alpha(\varepsilon_i(t))]\Big[\Big(\hat{\varepsilon}'(t) - \hat{\varepsilon}'_p(t)\Big) - \int_0^\infty \Gamma(\upsilon)p(\upsilon)d\upsilon\int_0^t \exp(-\Gamma(\upsilon)(t-\tau)) \times \Big(\hat{\varepsilon}'(\tau) - \hat{\varepsilon}'_p(\tau)\Big)d\tau\Big], \quad (22)$$

where P is an unknown pressure, $\hat{I}$ is the unit tensor, and

$$G = \frac{1}{2}\rho\mu N$$

is an analog of the shear modulus. The first term on the right-hand side of Eq. (22) arises due to the incompressibility condition. Substitution of Eq. (3) into Eq. (22) implies that

$$\hat{\sigma}(t) = -P(t)\hat{I} + 2G[1-\alpha(\varepsilon_i(t))]\Big[\Big(\hat{\varepsilon}'(t) - \hat{\varepsilon}'_p(t)\Big) - \gamma\int_0^\infty \exp(-\upsilon)p(\upsilon)d\upsilon\int_0^t \exp(-\gamma\exp(-\upsilon)(t-\tau)) \times \Big(\hat{\varepsilon}'(\tau) - \hat{\varepsilon}'_p(\tau)\Big)d\tau\Big]. \quad (23)$$

To approximate experimental data, we adopt a random energy model [46] with the quasi-Gaussian distribution function

$$p(\upsilon) = p_0\exp\Big[-\frac{(\upsilon - V)^2}{2\Sigma^2}\Big] \ (\upsilon \geqslant 0), \quad p(\upsilon) = 0 (\upsilon < 0), \quad (24)$$

where V is the dimensionless average energy for rearrangement of MRs, Σ is the dimensionless standard deviation of activation energies, and the coefficient p_0 is found from the condition

$$\int_0^\infty p(\upsilon)d\upsilon = 1. \quad (25)$$

For an arbitrary three-dimensional deformation with small strains, the time-dependent response of a polymer composite is determined by Eqs. (l0)–(13), (23) and (24). These equations involve five material constants:

1. the shear modulus G;
2. the strain, ε_*, that characterizes transition to a developed flow of MRs;
3. the attempt rate, γ, for rearrangement of meso-domains;
4. the average activation energy, V
5. the standard deviation of activation energies, Σ.

The number of adjustable parameters in the constitutive equations is noticeably less than that in other models for the viscoelastic and viscoplastic response of solid polymers [47–51].

Our aim now is to simplify the stress–strain relations for uniaxial tension and simple shear of an incompressible material.

6. Umaxial tension of a specimen

For uniaxial tension of an incompressible medium, the strain tensor reads

$$\hat{\varepsilon}(t) = \varepsilon(t)\Big[\bar{e}_1\bar{e}_1 - \frac{1}{2}(\bar{e}_2\bar{e}_2 + \bar{e}_3\bar{e}_3)\Big], \quad (26)$$

where $\varepsilon(t)$ is a longitudinal strain, and $\bar{e}_m (m = 1, 2, 3)$ are unit vectors of a Cartesian coordinate frame. The plastic strain tensor is assumed to be determined by the equation similar to Eq. (26),

$$\hat{\varepsilon}_p(t) = \varepsilon_p(t)\Big[\bar{e}_1\bar{e}_1 - \frac{1}{2}(\bar{e}_2\bar{e}_2 + \bar{e}_3\bar{e}_3)\Big], \quad (27)$$

where $\varepsilon_p(t)$ is an unknown function. It follows from Eqs. (26) and (27) that

$$\hat{\varepsilon}' = \hat{\varepsilon}, \quad \hat{\varepsilon}'_p = \hat{\varepsilon}_p. \quad (28)$$

Combining Eqs. (11) and (12) with Eqs. (26)–(28), we find that

$$\varepsilon_i(t) = \big|\varepsilon(t) - \varepsilon_p(t)\big|. \quad (29)$$

Substitution of Eqs. (26)–(28) into Eqs. (10) and (13) results in the kinetic equation

$$\frac{d\varepsilon_p}{dt} = \Big[1 - \exp\Big(-\frac{|\varepsilon - \varepsilon_p|}{\varepsilon_*}\Big)\Big]\frac{d\varepsilon}{dt}, \quad \varepsilon_p(0) = 0. \quad (30)$$

It follows from Eqs. (22) and (26)–(28) that the stress tensor, $\hat{\sigma}$, is given by

$$\hat{\sigma}(t) = \sigma(t)\bar{e}_1\bar{e}_1 + \sigma_0(t)(\bar{e}_2\bar{e}_2 + \bar{e}_3\bar{e}_3),$$

where

$$\sigma(t) = -P(t) + 2G[1-\alpha(\varepsilon_i(t))]\Big[\big(\varepsilon(t) - \varepsilon_p(t)\big) - \int_0^\infty \Gamma(\upsilon)p(\upsilon)d\upsilon\int_0^t \exp(-\Gamma(\upsilon)(t-\tau)) \times \big(\varepsilon(\tau) - \varepsilon_p(\tau)\big)d\tau\Big],$$

$$\sigma_0(t) = -P(t) - G[1-\alpha(\varepsilon_i(t))]\Big[\big(\varepsilon(t)-\varepsilon_p(t)\big) - \int_0^\infty \Gamma(\upsilon)p(\upsilon)d\upsilon\int_0^t \exp(-\Gamma(\upsilon)(t-\tau)) \times \big(\varepsilon(\tau)-\varepsilon_p(\tau)\big)d\tau\Big].$$

Excluding pressure, P, from the boundary condition on the lateral surface of a specimen, $\sigma_0(t)=0$, we find the longitudinal stress

$$\sigma(t) = E\,[1-\alpha(\varepsilon_i(t))]\Big[\big(\varepsilon(t)-\varepsilon_p(t)\big) - \int_0^\infty \Gamma(\upsilon)p(\upsilon)d\upsilon \times \int_0^t \exp(-\Gamma(\upsilon)(t-\tau))\big(\varepsilon(\tau)-\varepsilon_p(\tau)\big)d\tau\Big], \tag{31}$$

where

$$E = 3G \tag{32}$$

is Young's modulus. Eq. (31) is satisfied for an arbitrary deformation program. For rapid loading, when the viscoelastic phenomena may be disregarded, we combine Eqs. (29) and (31) and arrive at the stress–strain relation

$$\sigma = E\exp\left(-\frac{|\varepsilon-\varepsilon_p|}{\varepsilon_*}\right)\big(\varepsilon-\varepsilon_p\big). \tag{33}$$

Eqs. (30) and (33) will be employed in Section 8 to match observations in tensile tests with a constant strain rate.

7. Shear of a specimen

For shear of an incompressible medium, the strain tensor reads

$$\hat{\varepsilon}(t) = \varepsilon(t)(\bar{e}_1\bar{e}_2 + \bar{e}_2\bar{e}_1), \tag{34}$$

where $\varepsilon(t)$ is a shear strain. The plastic strain tensor is given by the equation similar to Eq. (34),

$$\hat{\varepsilon}_p(t) = \varepsilon_p(t)(\bar{e}_1\bar{e}_2 + \bar{e}_2\bar{e}_1), \tag{35}$$

where $\varepsilon_p(t)$ is a function to be found. It follows from Eqs. (34) and (35) that conditions (28) are satisfied. Combining Eqs. (11), (12), (34) and (35), we find that

$$\varepsilon_i = \frac{2}{\sqrt{3}}|\varepsilon-\varepsilon_p|. \tag{36}$$

Substitution of expressions (13) and (34)–(36) into Eq. (10) results in the kinetic equation

$$\frac{d\varepsilon_p}{dt} = \left[1-\exp\left(-\frac{2|\varepsilon-\varepsilon_p|}{\varepsilon_*\sqrt{3}}\right)\right]\frac{d\varepsilon}{dt}, \quad \varepsilon_p(0)=0. \tag{37}$$

It follows from Eqs. (13), (22), (28) and (34)–(36) that the shear stress, σ, reads

$$\sigma(t) = 2G\exp\left(-\frac{2|\varepsilon(t)-\varepsilon_p(t)|}{\varepsilon_*\sqrt{3}}\right)\Big[\big(\varepsilon(t)-\varepsilon_p(t)\big) - \int_0^\infty \Gamma(\upsilon)p(\upsilon)d\upsilon\int_0^t \exp(-\Gamma(\upsilon)(t-\tau)) \times \big(\varepsilon(\tau)-\varepsilon_p(\tau)\big)d\tau\Big]. \tag{38}$$

Eqs. (37) and (38) describe the time-dependent response of a polymer composite for an arbitrary program of shear with small strains. To fit experimental data in oscillatory torsion tests, we concentrate on shearing with a small amplitude of deformation,

$$|\varepsilon(t)| \ll \varepsilon_*. \tag{39}$$

Under this condition, kinetic Eq. (37) implies that

$$\varepsilon_p(t) = 0,$$

whereas Eq. (38) reads

$$\sigma(t) = 2G\Big[\varepsilon(t) - \int_0^\infty \Gamma(\upsilon)p(\upsilon)d\upsilon \times \int_0^t \exp(-\Gamma(\upsilon)(t-\tau))\varepsilon(\tau)d\tau\Big]. \tag{40}$$

We confine ourselves to a standard dynamic test with

$$\varepsilon(t) = \varepsilon_0\exp(i\omega t),$$

where ε_0 and ω are the amplitude and frequency of oscillations, and $i=\sqrt{-1}$. It follows from Eq. (40) that the transient complex modulus,

$$\bar{G}^*(t,\omega) = \frac{\sigma(t)}{2\varepsilon(t)},$$

is given by

$$\bar{G}^*(t,\omega) = G\left\{1 - \int_0^\infty \Gamma(\upsilon)p(\upsilon)d\upsilon\int_0^t \exp[-(\Gamma(\upsilon)+i\omega)s]ds\right\}, \tag{41}$$

where $s=t-\tau$. The steady-state complex modulus, $G^*(\omega)$, is defined as the limit of $\bar{G}^*(t,\omega)$ when t approaches infinity. Eq. (41) implies that

$$G^*(\omega) = G\int_0^\infty \frac{i\omega}{\Gamma(\upsilon)+i\omega}p(\upsilon)d\upsilon.$$

It follows from this equality and Eq. (3) that the steady-state storage, $G'(\omega)$, and loss, $G''(\omega)$, shear moduli read

$$G'(\omega) = G\int_0^\infty \frac{\omega^2}{\gamma^2\exp(-2\upsilon)+\omega^2}p(\upsilon)d\upsilon,$$

$$G''(\omega) = G\int_0^\infty \frac{\gamma\exp(-\upsilon)\omega}{\gamma^2\exp(-2\upsilon)+\omega^2}p(\upsilon)d\upsilon, \quad (42)$$

where the distribution function, $p(\upsilon)$, is determined by Eq. (24). Eqs. (24) and (42) will be employed in Section 8 to match observations in oscillatory torsion tests.

8. Fitting of observations

We begin with the approximation of the stress–strain curves for virgin polycarbonate depicted in Fig. 1. As the stress relaxation is negligible during the tensile tests, constitutive Eqs. (30) and (33) are applied to match the experimental data.

Each stress–strain curve presented in Fig. 1 is fitted independently. To find the constants, E and ε_*, in Eqs. (30) and (33), we fix an interval $[0, \varepsilon_{max}]$, where the "best-fit" parameter ε_* is assumed to be located, and divide this interval into J subintervals by the points $\varepsilon^{(i)} = i\Delta\varepsilon (i = 1, \ldots, J-1)$ with $\Delta\varepsilon = \varepsilon_{max}/J - 1$. For any $\varepsilon^{(i)}$ the governing equations are integrated numerically (with the step $\Delta\varepsilon = 1.0\times10^{-5}$) by the Runge–Kutta method. The elastic modulus, E, is found by the least-squares algorithm from the condition of minimum of the function

$$F = \sum_{\varepsilon_m}\left[\sigma_{exp}(\varepsilon_m) - \sigma_{num}(\varepsilon_m)\right]^2,$$

where the sum is calculated over all experimental points, ε_m, depicted in Fig. 1, σ_{exp} is the longitudinal stress measured in a tensile test, and σ_{num} is given by Eq. (33). The "best-fit" parameter, ε_*, minimizes the cost function, F, on the set $\{\varepsilon^{(i)}(i = 1\ldots, J-1)\}$. After determining the "best-fit" value, $\varepsilon^{(i)}$ this procedure is repeated twice for the new interval $[\varepsilon^{(i-1)},\varepsilon^{(i+1)}]$, to ensure an acceptable accuracy of matching observations. Fig. 1 demonstrates fair agreement between the experimental data and the results of numerical simulation for all concentrations of short glass fibers, ϕ, under consideration.

Afterwards, the same procedure of fitting observations is applied to match the experimental data in tensile tests on recycled polycarbonate and on the mixture of virgin and recycled polymers plotted in Figs. 2 and 3.

The "best-fit" parameters, E and ε, are presented in Figs. 10 and 11 as functions of the content, ϕ, of short glass fibers.

The experimental data for Young's modulus for all three types of polymer composites are approximated by the linear function

$$E = E_0 + E_1\phi, \quad (43)$$

where the coefficients, E_0 and E_1, are found by the least-squares technique. Fig. 10 demonstrates good agreement between the observations and their description by Eq. (43).

For each type of the polymer composite, the experimental data for the strain, ε_*, are approximated by the linear function

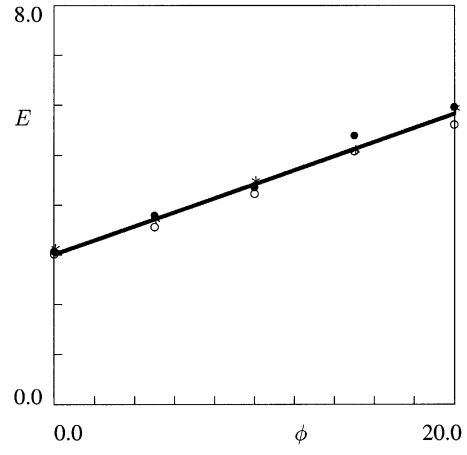

Fig. 10. The Young modulus E GPa versus the content of short glass fibers ϕ wt.%. Symbols: treatment of observations in tensile tests on virgin (unfilled circles), recycled (filled circles) and mixture of virgin and recycled (asterisks) polycarbonates. Solid line: approximation of the experimental data by Eq. (43) with $E_0 = 3.01$ and $E_1 = 0.14$.

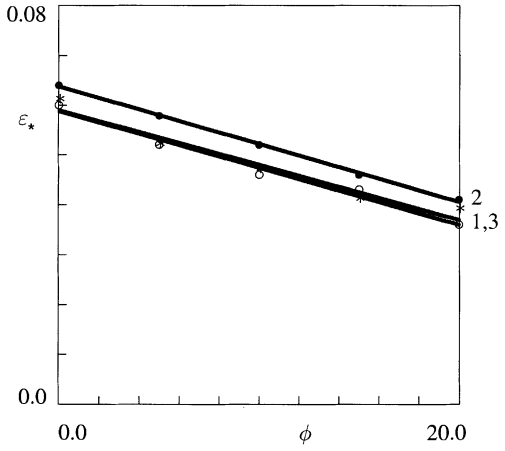

Fig. 11. The strain ε_* that characterizes transition to a developed plastic flow versus the content of short glass fibers ϕ wt.%. Symbols: treatment of observations in tensile tests on virgin (unfilled circles), recycled (filled circles) and mixture of virgin and recycled (asterisks) polycarbonates. Solid lines: approximation of the experimental data by Eq. (44). Curve 1: $\varepsilon_0 = 5.88\times10^{-2}$, $\varepsilon_1 = 1.14\times10^{-3}$. Curve 2: $\varepsilon_0 = 6.38\times10^{-2}$, $\varepsilon_1 = 1.16\times10^{-2}$. Curve 3: $\varepsilon_0 = 5.90\times10^{-2}$, $\varepsilon_1 = 1.10\times10^{-3}$.

$$\varepsilon_* = \varepsilon_0 - \varepsilon_1\phi, \tag{44}$$

where the coefficients, ε_0 and ε_1, are determined by the least-squares method. Fig. 11 demonstrates that Eq. (44) correctly describes a decrease in ε_* with the filler content. For any concentration of glass fibers, ϕ, the strain for transition to a developed flow of junctions, ε_*, for recycled polycarbonate slightly exceeds that for virgin polycarbonate, whereas there is practically no difference between the values of ε_* for virgin polymer and the mixture of virgin and recycled polycarbonates.

We proceed with the approximation of the experimental data in dynamic tests depicted in Figs. 4–9. According to Fig. 11, the strain, ε_*, that characterizes transition to a steady flow of junctions belongs to the interval between 3 and 7%, which means that inequality (39) is satisfied for sinusoidal oscillations with an amplitude of 0.1%. This implies that Eqs. (24) and (42) may be applied to fit the observations.

Each set of experimental data for the storage, $G'(\omega)$, and loss, $G''(\omega)$, moduli is matched independently. To find the material constants, G, γ, V and Σ, in governing Eqs. (24) and (42), we apply an algorithm similar to that employed to fit observations in tensile tests. First, the experimental data for virgin polycarbonate (Figs. 4 and 5) are approximated. We begin with the experimental data for neat polymer ($\phi = 0.0$), fix some intervals, $[0, \gamma_{\max}]$, $[0, V_{\max}]$ and $[0, \Sigma_{\max}]$, where the "best-fit" parameters γ, V and Σ are assumed to be located, and divide these intervals into J subintervals by the points $\gamma^{(i)} = i\Delta\gamma$, $V^{(j)} = j\Delta V$ and $\Sigma^{(k)} = k\Delta\Sigma (i, j, k = 1, \ldots, J-1)$ with $\Delta\gamma = \gamma_{\max}/J$, $\Delta V = V_{\max}/J$ and $\Delta\Sigma = \Sigma_{\max}/J$. For any pair, $\{V^{(j)}, \Sigma^{(k)}\}$ the coefficient, p_0 in Eq. (24) is found from condition (25), where the integral is calculated numerically by Simpson's method with 200 points and the step $\Delta\upsilon = 0.5$. For any triple, $\{\gamma^{(i)}, V^{(j)}, \Sigma^{(k)}\}$, the integrals in Eq. (42) are evaluated numerically. The coefficient $G = G(i,j,k)$ is determined by the least-squares technique from the condition of minimum of the function

$$F = \sum_{\omega_m} \left\{ \left[G'_{\exp}(\omega_m) - G'_{\text{num}}(\omega_m) \right]^2 + \eta \left[G''_{\exp}(\omega_m) - G''_{\text{num}}(\omega_m) \right]^2 \right\},$$

where the sum is calculated over all frequencies, ω_m, in the oscillatory tests, $G'_{\exp}$, $G''_{\exp}$ are the storage and loss moduli measured in the steady-state dynamic test, and G'_{num}, G''_{num} are given by Eq. (42). As the storage modulus, $G'_{\exp}$, exceeds the lost modulus, $G''_{\exp}$, by two orders of magnitude, we set $\eta = 5000.0$ in the expression for the cost function, F. The parameters γ, V and Σ are determined from the condition of minimum of the function F on the set $\{\gamma^{(i)}, V^{(j)}, \Sigma^{(k)} \quad (i, j, k = 1, \ldots, J-1)\}$. After finding the "best-fit" values, $\gamma^{(i)}$, $V^{(j)}$ and $\Sigma^{(k)}$, the approximation procedure is repeated twice for the new intervals $[\gamma^{(i-1)}, \gamma^{(i+1)}]$, $[V^{(j-1)}, V^{(j+1)}]$ and $[\Sigma^{(k-1)}, \Sigma^{(k+1)}]$, to ensure an acceptable accuracy of fitting.

Table 1
The attempt rate γ s^{-1} for polymer composites with various matrices

Matrix	γ
Virgin	78
Mixture	770
Recycled	21 000

To match the observations in dynamic tests on filled polycarbonate, $\phi > 0$, we fix the attempt rate, γ, found in the approximation of experimental data for the neat polymer, and apply the above algorithm of fitting with only three adjustable parameters, G, V and Σ.

Afterwards, the same procedure of fitting observations is applied to observations on recycled polycarbonate (Figs. 6 and 7) and mixture of virgin and recycled polycarbonates (Figs. 8 and 9). Figs. 4–9 show excellent agreement between the experimental data and the results of numerical simulation.

The attempt rates, γ, for three types of polymer composites are listed in Table 1.

The shear modulus, G, is plotted versus the filler content, ϕ, in Fig. 12. The experimental data are approximated by the linear function similar to Eq. (43) employed in matching observations in tensile tests with a constant strain rate,

$$G = G_0 + G_1\phi. \tag{45}$$

The coefficients, G_0 and G_1, in Eq. (45) are found by the least-squares technique. Fig. 12 demonstrates that Eq. (45) correctly describes the effect of concentration of

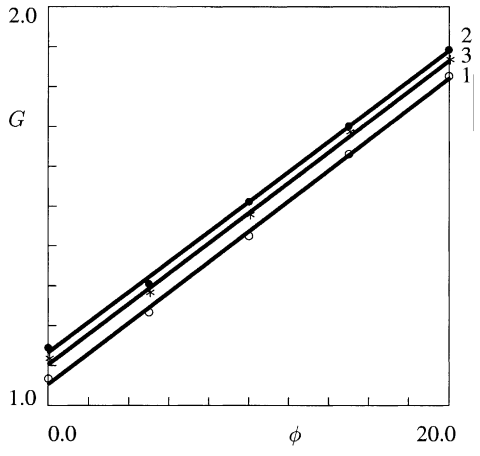

Fig. 12. The shear modulus G GPa versus the content of short glass fibers ϕ wt.%. Symbols: treatment of observations in oscillatory torsion tests on virgin (unfilled circles), recycled (filled circles) and mixture of virgin and recycled (asterisks) polycarbonates. Solid lines: approximation of the experimental data by Eq. (45). Curve 1: $G_0 = 1.05$, $G_1 = 3.83\times10^{-2}$. Curve 2: $G_0 = 1.13$, $G_1 = 3.78\times10^{-2}$. Curve 3: $G_0 = 1.10$, $G_1 = 3.80\times10^{-2}$.

short glass fibers, ϕ, on the shear modulus for all types of polymer composites.

The adjustable parameters, V and Σ, are plotted versus the content of glass fibers, ϕ, in Figs. 13 and 14. The experimental data are approximated by the linear functions

$$V = V_0 + V_1\phi, \quad \Sigma = \Sigma_0 + \Sigma_1\phi, \tag{46}$$

where the coefficients, V_m and Σ_m ($m=0,1$), are determined by the least-squares method. Figs. 13 and 14 show that Eqs. (46) adequately predict the effect of filler on the average energy, V, for rearrangement of meso-regions, and the standard deviation of activation energies, Σ.

To compare Young's modulus, E, found in tensile tests with a constant strain rate, with the shear modulus, G, determined in oscillatory torsion tests, we plot the quantities, $\frac{1}{3}E$ and G, determined for composites with recycled matrices versus the filler content, ϕ, in Fig. 15. According to the incompressibility condition, the amounts, $\frac{1}{3}E$ and G, coincide, see Eq. (32). Fig. 15, where the observations are presented together with their approximation by Eq. (45), shows that the incompressibility condition is satisfied with a high level of accuracy. It is worth noting that Eq. (32) is fulfilled with the same accuracy for polymer composites with virgin matrices and for the mixture of virgin and recycled polycarbonates (for the sake of brevity, appropriate figures are omitted). These observations validate our treatment of polymer composites as ensembles of incompressible meso-regions. The above conclusion does not contradict the conventionally accepted fact that polycarbonate at ambient temperature is a compressible material whose Poisson's ratio ranges from 0.40 to 0.45 [52]. The difference between our approach and the conventional one is that the elastic modulus, E, is found by matching the entire stress–strain diagrams up to the strains corresponding to the onset of necking, whereas Young's modulus is traditionally determined by fitting an initial part of a stress–strain curve only. This implies that E should slightly exceed conventional Young's modulus (for virgin polycarbonate E is higher than the Young modulus provided by the supplier by 39%).

It is worth noting that Eq. (32) is grounded on the assumption that the equivalent network is isotropic. The presence of short glass fibers in injection-molded specimens may result in an anisotropy of the network,

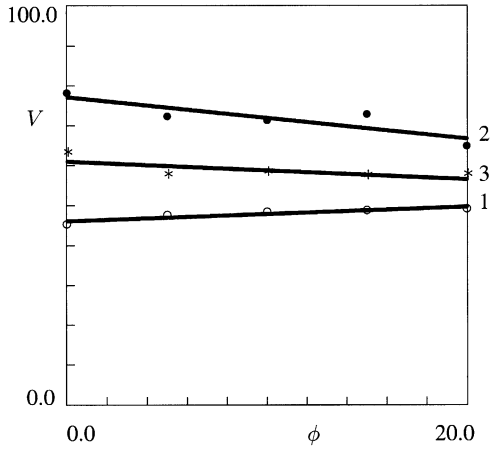

Fig. 13. The average activation energy V versus the content of short glass fibers ϕ wt.%. Symbols: treatment of observations in oscillatory torsion tests on virgin (unfilled circles), recycled (filled circles) and mixture of virgin and recycled (asterisks) polycarbonates. Solid lines: approximation of the experimental data by Eq. (46). Curve 1: $V_0=46.06$, $V_1=0.18$. Curve 2: $V_0=77.12$, $V_1=-0.52$. Curve 3: $V_0=60.92$, $V_1=-0.22$.

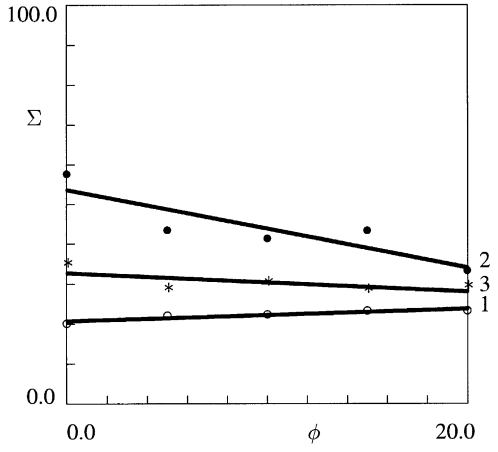

Fig. 14. The standard deviation of activation energies Σ versus the content of short glass fibers ϕ wt.%. Symbols: treatment of observations in oscillatory torsion tests on virgin (unfilled circles), recycled (filled circles) and mixture of virgin and recycled (asterisks) polycarbonates. Solid lines: approximation of the experimental data by Eq. (46). Curve 1: $\Sigma_0=20.72$, $\Sigma_1=0.15$. Curve 2: 53.64, $\Sigma_1=-0.98$. Curve 3: $\Sigma_0=32.74$, $\Sigma_1,=-0.23$.

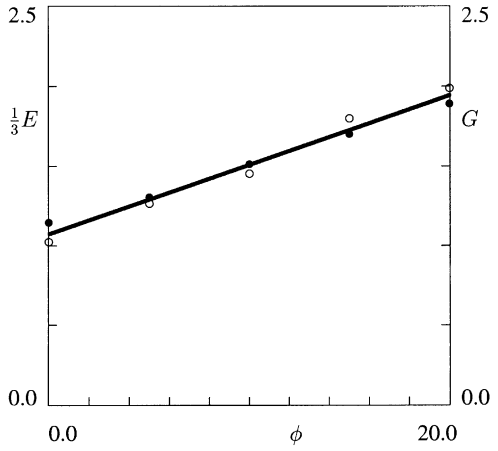

Fig. 15. The Young modulus E GPa (unfilled circles) and the shear modulus G GPa (filled circles) versus the content of short glass fibers ϕ wt.%. Symbols: treatment of observations in tensile tests and oscillatory torsion tests on recycled polycarbonate. Solid line: approximation of the experimental data by Eq. (45) with $G_0=1.07$ and $G_1=4.36\times10^{-2}$.

but the coincidence of the moduli, $\frac{1}{3}E$ and G, indicates that this anisotropy may be disregarded.

9. Discussion

According to Figs. 10 and 12, the Young modulus, E, and the shear modulus, G, linearly grow with the content of filler, ϕ. A linear increase in the elastic moduli of polymer composites with concentration of short glass fibers has previously been reported in several studies [21,24,27,29]. This growth is attributed to the fact that the rigidity of short glass fibers substantially exceeds the shear moduli of the host matrices. Fig. 10 demonstrates small and inconsistent deviations between Young's moduli of virgin, recycled and the mixture of virgin and recycled polycarbonates reinforced with glass fibers. Fig. 12 confirms this conclusion, but reveals that these deviations are consistent: the shear modulus of the recycled polycarbonate exceeds that for the mixture of virgin and recycled polymers, which, in turn, exceeds the shear modulus of virgin polycarbonate. We suppose that the experimental data depicted in Fig. 12 characterize the influence of recycling on the elastic modulus of the composites more adequately. Inconsistent deviations of Young's modulus presented in Fig. 10 may be explained by the fact that the length of specimens for tensile tests exceeds that of samples for torsion tests about by twice, which implies highly irregular distribution of impurities.

Fig. 11 shows that the strain, ε_*, that characterizes transition to a developed flow of junctions decreases with the content of filler, ϕ. This observations seems quite natural, and may be attributed to the following processes at the micro-level:

1. Short glass fibers serve as local stress concentrators in polymer composites, around which viscoplastic deformation occurs in the host matrix. This means that given a macro-strain, ε, the higher the content of filler is, the larger is the number of meso-domains that slide with respect to surrounding regions. This conclusion is reflected by a decrease in the coefficient, ε_*, in Eqs. (10) and (13).
2. As adhesion between short glass fibers and the polymer matrix is rather weak (compared with the strength of interaction between chains in neat polycarbonate), viscoplastic flow of meso-regions is initiated at the surfaces of filler particles, which implies that an increase in the content of fibers is tantamount to the growth of the intensity of viscoplastic flow.

The fact that an increase in the content of glass fibers enhances the viscoplastic flow is confirmed by the experimental data depicted in Figs. 1–3, which show that the higher the content of fibers is, the smaller is the strain at which spatially homogeneous deformation of specimens is transformed into heterogeneous deformation and formation of a neck.

Fig. 11 reveals that for any content of fibers, ϕ, the strain, ε_*, for recycled polycarbonate slightly exceeds that for virgin polycarbonate and the mixture of virgin and recycled polycarbonates, which is in agreement with observations for the shear modulus, G, depicted in Fig. 12. These small, but consistent, differences in the values of G and ε_* may be attributed to chemical degradation (thermo-oxidative aging) of post-consumer plastic waste [20], which is conventionally associated with scission of polymeric chains [53]. Short chains created during the thermo-oxidative process serve as extra cross-links in the recycled polymer. The presence of these additional cross-links increases the elastic modulus (which is proportional to the number of active strands in a polymeric network) and enhances resistance to sliding of meso-domains with respect to each other (because these short chains form extra links between meso-regions). This conclusion is confirmed by differential scanning calorimetry (DSC) measurements [15] that suggest a decrease in the glass transition temperature of a mixture of virgin and recycled polymers (which is tantamount to a reduction of molecular mobility) with the growth of the content of recycled material.

Fig. 13 demonstrates that the average activation energy for rearrangement of meso-regions, V, weakly grows with the content of short glass fibers, ϕ, for virgin polycarbonate, and slightly decreases with ϕ for recycled polycarbonate and the mixture of virgin and recycled polymers. For any content of glass fibers, ϕ, the average activation energy, V, for polymer composites with recycled matrices substantially exceeds that for the mixture of virgin and recycled polymers, which, in turn, is larger than the average activation energy of composites with virgin matrices. The latter conclusion may be ascribed to the presence of short chains in recycled polycarbonate that serve as extra links between meso-regions which prevent their rearrangement.

A slight increase in the average average activation energy of MRs in composites with virgin matrices driven by the growth of the content of short glass fibers (curve 1 in Fig. 13) may be explained within the shoving concept [54,55]. According to this approach, rearrangement of a meso-region requires an instantaneous local increase in volume that takes place when surrounding chains are shoved aside due to thermal excitations. The latter means that the potential energy of a trap, υ, equals the sum of two components: the energy of thermal fluctuations necessary for rearrangement of strands in an individual MR and the mechanical energy for shoving aside surrounding domains. The first quantity is independent of the content of filler, and it is entirely deter-

mined by temperature and topology of chains. The other contribution into the potential energy of traps (the work for shoving aside surrounding meso-domains) linearly increases with the shear modulus [54]. As the shear moduli of the polymer composites increase with the content of filler (Fig. 12), a similar growth is expected for the average activation energy of MRs, V, which is in agreement with the experimental data depicted in Fig. 13.

Curves 2 and 3 in Fig. 13 demonstrate that the shoving concept can serve only as one of possible mechanisms for changes in the average activation energy, V, driven by the presence of filler. Adhesion of polymeric chains on the surfaces of glass fibers provides another mechanism for the alteration of activation energies of MRs. It is natural to assume that the presence of impurities in the post-consumer plastic waste results in a pronounced decrease in the compatibility of recycled polycarbonate with glass fibers. As a result of this incompatibility, the energy of adhesion of polymeric chains on fibers is substantially reduced, which implies that these chains require rather low activation energy for their rearrangement. This implies that the higher the content of glass fibers is in a polymer composite, the lower is the average activation energy for rearrangement of meso-domains. With reference to this assertion, we suppose that the weak decrease in the average activation energies, V, of recycled polycarbonate and the mixture of virgin and recycled polycarbonates with ϕ observed in Fig. 13 may be attributed to the cumulative effect of two factors: (i) an increase in $V(\phi)$ in accord with the shoving model, and (ii) a decrease in $V(\phi)$ induced by weakening of adhesion of polymer chains on the surfaces of fibers.

According to Fig. 14, the standard deviation of activation energies, Σ, weakly increases with the content of filler, ϕ, for virgin polycarbonate and decreases for recycled polycarbonate and for the mixture of virgin and recycled polymers. For any concentration of glass fibers, ϕ, the standard deviation of activation energies is maximal for recycled polycarbonate and minimal for virgin polymer.

The fact that Σ for recycled polycarbonate exceeds that for the mixture of virgin and recycled polymers, which, in turn, exceeds the standard deviation of activation energies for virgin polycarbonate seems quite natural, if we recall that Σ serves as a measure of inhomogeneity in an ensemble of meso-domains, see Eq. (24). As the level of heterogeneity in the recycled polycarbonate is noticeably larger than that in virgin polymer (due to the presence of impurities), the standard deviation of activation energies in the composites with recycled matrices is higher as well.

The growth of Σ with ϕ (curve 1 in Fig. 14) reflects the fact that an increase in the filler content enhances heterogeneity of an ensemble of meso-domains in virgin polycarbonate. The latter is driven by the inhomogeneity of interactions between short glass fibers and the host matrix at the micro-level. The decrease in Σ with ϕ for recycled polycarbonate (curve 2 in Fig. 14) may be attributed to weakening of adhesive properties on the surfaces of glass fibers, which implies that MRs in an ensemble become more homogeneously distributed (because the "tail" of the distribution function $p(\upsilon)$ disappears corresponding to high activation energies, υ).

According to Figs. 13 and 14, the average activation energy, V, and the standard deviation of activation energies, Σ, are pronouncedly altered with an increase in the content of glass fibers, ϕ. However, the width of the distribution of meso-regions, characterized by the ratio,

$$\xi = \frac{\Sigma}{V},$$

remains practically independent of the filler fraction.

Table 1 demonstrates that the attempt rate for rearrangement of meso-domains, γ, is minimal for virgin polycarbonate, it is maximal for recycled polymer, whereas γ for the mixture of virgin and recycled polycarbonates is intermediate between those for virgin and recycled polymers. This conclusion is in agreement with our previous study [56] on the viscoelastic behavior of melts of virgin and recycled polycarbonates, which shows that recycling of polycarbonate enhances molecular mobility of the melts. An increase in γ after recycling may be attributed to pronounced weakening of interactions between polymeric chains driven by scission of macromolecules (thermo-oxidative degradation).

10. Concluding remarks

Three series of tensile tests with a constant strain rate and oscillatory torsion tests have been performed at room temperature on polymer composites with polycarbonate matrices reinforced with various amounts of short glass fibers. In the first series of tests, virgin polycarbonate was used, whereas in the other series, recycled polycarbonate and a mixture of virgin and recycled polymers were employed as the host matrix.

A model has been developed for the viscoelastic and viscoplastic responses of a polymer composite at isothermal deformation with small strains. A complicated micro-structure of a composite is replaced by an equivalent ensemble of meso-regions with various activation energies for their rearrangement. The viscoelastic behavior is attributed to rearrangement of MRs. The rearrangement events occur at random times when meso-domains are excited by thermal fluctuations. The viscoplastic behavior is associated with sliding of

meso-regions with respect to each other. The rate of sliding is proportional to the rate of macro-strain.

Constitutive equations have been derived for the time-dependent response of polymer composites at three-dimensional deformation by using the laws of thermodynamics. The stress–strain relations involve five adjustable parameters that are found by fitting the experimental data. Fair agreement is demonstrated between the observations and the results of numerical simulation.

The following conclusions are drawn:

1. The Young modulus, E, and the shear modulus, G, of a polymer composite linearly increase with the filler content, ϕ.
2. The strain, ε_*, that characterizes transition to a steady flow of meso-domains decreases with ϕ.
3. The elastic moduli and the strain for transition to a developed viscoplastic flow are weakly affected by the type of host matrix.
4. The average activation energy for rearrangement, V, and the standard deviation of activation energies, Σ, are the largest for recycled polycarbonate and the smallest for virgin polycarbonate. These parameters, as well as the attempt rate for rearrangement of MRs, γ, are strongly affected by the type of polymeric matrix.
5. With an increase in the content, ϕ, of short glass fibers, V and Σ slightly grow for virgin polycarbonate (which may be explained within the shaving concept), and weakly decrease for recycled polymer and the mixture of virgin and recycled polycarbonates (which is associated with weakening of adhesion of polymeric chains in host matrices with impurities on the surfaces of short glass fibers).

Summing up these observations, we conclude that recycling of polycarbonate weakly affects the viscoplastic behavior of polymer composites filled with short glass fibers, but noticeably influences their viscoelastic response.

Acknowledgements

This work was partially supported by the US Department of Energy through grant DE-FC26-00FT40598.

References

[1] Eriksson P-A, Boydell F, Eriksson K, Manson J-AE, Albertsson A-C. Effect of thermal-oxidative aging on mechanical, chemical, and thermal properties of recycled polyamide 66. J Appl Polym Sci 1997;65:1619–30.

[2] Wenguang M, La Mantia FP. Processing and mechanical properties of recycled PVC and of homopolymer blends with virgin PVC. J Appl Polym Sci 1998;59:759–67.

[3] Albano C, Sanchez G. Study of the mechanical, thermal, and thermodegradative properties of virgin PP with recycled and non-recycled HDPE. Polym Eng Sci 1999;39:1456–62.

[4] Arnold JC, Maund B. The properties of recycled PVC bottle compounds. 1: Mechanical performance. Polym Eng Sci 1999;39: 1234–41.

[5] Incarnato L, Scarfato P, Acierno D. Rheological and mechanical properties of recycled polypropylene. Polym Eng Sci 1999;39: 749–55.

[6] Incarnato L, Scarfato P, Gorrasi G, Vittoria V, Acierno D. Structural modifications induced by recycling of polypropylene. Polym Eng Sci 1999;39:1661–6.

[7] La Mantia FP. Mechanical properties of recycled polymers. Macromol Symp 1999;147:167–72.

[8] Liu X, Bertilsson H. Recycling of ABS and ABS/PC blends. J Appl Polym Sci 1999;74:510–5.

[9] Michael H, Scholz H, Mennig G. Blends from recycled rubber and thermoplastics. Kautsch Gummi Kunst 1999;52:510–3.

[10] Bliznakov ED, White CC, Shaw MT. Mechanical properties of blends of HDPE and recycled urea-formaldehyde resin. J Appl Polym Sci 2000;77:3220–7.

[11] Ciesielska D, Liu P. Mechanical, rheological and morphological properties of recycled expanded polystyrene/styrene butadiene rubber blends. Kautsch Gummi Kunst 2000;53:273–8.

[12] Popovska-Pavlovska F, Trajkovska A, Trajkovska A, Gavrilov T. Rhealogical behaviour of VPVC/RPVC blends. Macromol Symp 2000;149:191–5.

[13] Bonelli CMC, Martins AF, Mano EB, Beatty CL. Effect of recycled polypropylene on polypropylene/high-density polyethylene blends. J Appl Polym Sci 2001;80:1305–11.

[14] Miller P, Sbarski I, Iovenitti P, Masood S, Kosior E. Rheological properties of blends of recycled HDPE and virgin polyolefins. Polym Recycling 2001;6:181–6.

[15] Sombatsompop N, Thongsang S. Rheology, morphology, and mechanical and thermal properties of recycled PVC pipes. J Appl Polym Sci 2001;82:2478–86.

[16] Bertin S, Robin JJ. Study and characterization of virgin and recycled LDPE/PP blends. Eur Polym J 2002;38:2255–64.

[17] Pracella M, Rolla L, Chionna D, Galeski A. Compatibilization and properties of poly(ethylene terephthalate)/polyethylene blends based on recycled materials. Macromol Chem Phys 2002; 203:1473–85.

[18] Xu G, Qiao J, Kuswanti C, Koelling K, Stuart JA, Lilly B. Characterization of virgin and postconsumer blended high-impact polystyrene resins for injection molding. J Appl Polym Sci 2002;84:1–8.

[19] Wyser Y, Leterrier Y, Manson J-AE. Effect of inclusions and blending on the mechanical performance of recycled multilayer PP/PET/SiO_x films. J Appl Polym Sci 2000;2000:910–8.

[20] Luda MP, Ragosta O, Musto P, Pollicino A, Camino O, Recca A, Nepote V. Natural ageing of automotive polymer components: characterisation of new and used poly(propylene) based car bumpers. Macromol Mater Eng 2002;287:404–11.

[21] Ha K-C, Hwang J-R, Doong J-L. Tensile properties of short glass fibre reinforced polycarbonate. Polym Polym Compos 1996; 4:563–76.

[22] Jang J, Lee JY, Jeong JK. Performance improvement of glass-fiber-reinforced polystyrene composite using a surface modifier. 2. Mechanical properties of composites. J Appl Polym Sci 1996; 59:2069–77.

[23] Kalaprasad G, Joseph K, Thomas S. Influence of short glass fiber addition on the mechanical properties of sisal reinforced low density polyethylene composites. J Compos Mater 1997;31:509–27.

[24] Kwok KW, Choy CL, Lau FR. Elastic moduli of injection-molded short-glass-fiber-reinforced poly(ethylene terephthalate). J Reinforced Plast Compos 1997;16:290–305.
[25] Hollin J, Miller D, Vautour D. A comparison of transverse properties of 50% short and long glass fiber reinforced nylon 6/6 resin. J Reinforced Plast Compos 1998;17:1617–24.
[26] Chishoim BJ, Fong PM, Zimmer JG, Hendrix R. Properties of glass-filled thermoplastic polyesters. J Appl Polym Sci 1999;74: 889–99.
[27] Lee SW, Youn JR. Characterization of short glass fiber filled polystyrene by fiber orientation and mechanical properties. Macromol Symp 1999;148:211–28.
[28] Patel KJ, Amin KG, Patel RG. Glass fiber-reinforced composites of diglycidyl ether of 2,7-dihydroxy naphthalene. J Appl Polym Sci 2000;75:1345–9.
[29] Cerrada ML, Benavente R, Perez E. Effect of short glass fiber on structure and mechanical behavior of an ethylene-1-octene copolymer. Macromol Chem Phys 2001;202:2686–95.
[30] Arencan D, Velasco JI. The influence of injection-molding variables and nucleating additives on thermal and mechanical properties of short glass fiber/PET composites. J Thermoplast Comp Mater 2002;15:317–36.
[31] Raval DK, Patel RB, Vyas SK. Fabrication and characterization of glass fiber reinforced composites from 2,3-epoxypropyl 3-(2-furyl) acrylate and acrylonitrile. Macromol Mater Engng 2002;287: 133–8.
[32] Tjong SC, Xu SA, Li RK, Mai YW. Mechanical behavior and fracture toughness evaluation of maleic anhydride compatibilized short glass fiber/SEBS/polypropylene hybrid composites. Compos Sci Technol 2002;62:831–40.
[33] Bergstrom JS, Kurtz SM, Rimnac CM, Edidin AA. Constitutive modeling of ultra-high molecular weight polyethylene under large-deformation and cyclic conditions. Biomaterials 2002;23: 2329–43.
[34] Adam O, Gibbs JH. On the temperature dependence of cooperative relaxation properties in glass-forming liquids. J Chem Phys 1965;43:139–46.
[35] Sollich P. Rheological constitutive equation for a model of soft glassy materials. Phys Rev E 1998;58:738–59.
[36] Mermet A, Duval E, Etienne S, G'Sell C. Effect of a plastic deformation on the nanostructure of polycarbonate: study by low-frequency Raman scattering. Polymer 1996;37:615–23.
[37] Arndt M, Stannarius R, Groothues H, Hempel E, Kremer F. Length scale of cooperativity in the dynamic glass transition. Phys Rev Lett 1997;79:2077–80.
[38] Rizos AK, Ngai KL. Experimental determination of the cooperative length scale of a glass-forming liquid near the glass transition temperature. Phys Rev E 1999;59:612–7.
[39] Drozdov AD, Christiansen J de C. The effect of annealing on the elastoplastic response of isotactic polypropylene. Eur Polym J 2003;39:21–31.
[40] O'Connell PA, McKenna GB. Arrhenius-type temperature dependence of the segmental relaxation below T_g. J Chem Phys 1999;110:11054–60.
[41] O'Connell PA, McKenna GB. The non-linear viscoelastic response of polycarbonate in torsion: an investigation of time-temperature and time-strain superposition. Mech Time-Dependent Mater 2002;6:207–29.
[42] Buchenau U. Mechanical relaxation in glasses and the glass transition. Phys Rev B 2001;63:104203.
[43] Goldstein M. Viscous liquids and the glass transition: a potential energy barrier picture. J Chem Phys 1969;51:3728–39.
[44] Bouchaud J-P, Cugliandolo LF, Kurchan J, Mezard M. Out of equilibrium dynamics in spin glasses and other glassy systems. In: Young AP, editor. Spin glasses and random fields. Singapore: World Scientific; 1998. p. 161–223.
[45] Men Y, Strobl O. Evidence for a mechanically active high temperature relaxation process in syndiotactic polypropylene. Polymer 2002;43:2761–8.
[46] Derrida B. Random-energy model: limit of a family of disordered models. Phys Rev Lett 1980;45:79–92.
[47] Bordonaro CM, Krempl E. A state variable model for high strength polymers. Polym Eng Sci 1995;35:310–6.
[48] Hasan OA, Boyce MC. A constitutive model for the nonlinear viscoelastic viscoplastic behavior of glassy polymers. Polym Eng Sci 1995;35:331–44.
[49] Sweeney J, Ward IM. A constitutive law for large deformations of polymers at high temperatures. J Mech Phys Solids 1996;44:1033–49.
[50] Boyce MC, Sacrate S, Llana PG. Constitutive model for the finite deformation stress-strain behavior of poly(ethylene terephthalate) above the glass transition. Polymer 2000;41:2183–201.
[51] Khan A, Zhang H. Finite deformation of a polymer: experiments and modeling. Int J Plasticity 2001;17:1167–88.
[52] Tschoegl NW, Knauss WG, Emri I. Poisson's ratio in linear viscoelasticity—a critical review. Mech Time-Dependent Mater 2002;6: 3–51.
[53] Stack S, O'Donoghue O, Birkinshaw C. The thermal stability and thermal degradation of blends of syndiotactic polystyrene and polyphenylene ether. Polym Degrad Stab 2003;79:29–36.
[54] Dyre JC. Source of non-Arrhenius average relaxation time in glass-forming liquids. J Non-Cryst Solids 1998;235–237:142–9.
[55] Olsen NB, Dyre JC, Christensen T. Structural relaxation monitored by instantaneous shear modulus. Phys Rev Lett 1998;81:1031–3.
[56] Drozdov AD, Al-Mulla A, Gupta RK. The viscoelastic behavior of melts of virgin and recycled polycarbonate reinforced with short glass fibers. Mech Research Comm (in press).